Cell width dictates Type VI secretion tail length

Yoann Santin, Thierry Doan, Laure Journet, Eric Cascales

Cell width dictates Type VI secretion tail length

Yoann G. Santin[1], Thierry Doan[1], Laure Journet[1] & Eric Cascales[1,2,*]

[1]Laboratoire d'Ingénierie des Systèmes Macromoléculaires, Institut de Microbiologie de la Méditerranée, Aix-Marseille Université – CNRS UMR7255, 31 Chemin Joseph Aiguier, CS7071, 13402 Marseille Cedex 09, France

[2]Lead Contact

[*]Correspondence: cascales@imm.cnrs.fr

Running title: T6SS sheath length control

Keywords : Protein transport, protein secretion, contractile injection systems, tail sheath, length regulation, TagA, cell width, molecular ruler, membrane.

SUMMARY

The type VI secretion system (T6SS) is a multiprotein apparatus that injects protein effectors into target cells, hence playing a critical role in pathogenesis and in microbial communities [1–4]. The T6SS belongs to the broad family of contractile injection systems (CIS), such as *Myoviridae* bacteriophages and R-pyocins, that use a spring-like tail to propel a needle loaded with effectors [5,6]. The T6SS tail comprises an assembly baseplate on which polymerizes a needle, made of stacked Hcp hexamers, tipped by the VgrG-PAAR spike complex and wrapped by the contractile sheath made of TssB and TssC [7–13]. The T6SS tail is anchored to the cell envelope by a membrane complex that also serves as channel for the passage of the needle upon sheath contraction [14–16]. In most CIS, the length of the tail sheath is invariable, and is usually ensured by a dedicated protein called tape measure protein (TMP) [17–22]. Here we show that the length of the T6SS tail is constant in enteroaggregative *Escherichia coli* cells, suggesting that it is strictly controlled. By overproducing T6SS tail subunits we demonstrate that component stoichiometry does not participate to the regulation of tail length. The observation of longer T6SS tails when the apparatus is relocalized at the cell pole further shows that tail length is not controlled by a TMP. Finally, we show that tail stops its elongation when in contact with the opposite membrane, and thus that T6SS tail length is determined by the cell width.

RESULTS AND DISCUSSION

T6SS tail sheath length in EAEC.

The length of bacteriophage and other CIS tails such as that of anti-feeding prophages is strictly controlled [17-23]. To determine whether this is also the case for the T6SS, we

40 measured the length of T6SS sheaths in EAEC wild-type cells producing a functional fusion
41 between the TssB tail subunit and the superfolder-Green Fluorescent Protein (TssB-sfGFP).
42 The sfGFP-coding sequence was inserted on the chromosome, upstream the *tssB* stop codon.
43 In this construct, the sfGFP sequence is in frame with the *tssB* gene, and the *tssB-sfGFP*
44 fusion is under the control of the native *tssB* expression signals. Cells were grown in *sci1*
45 inducing medium (SIM), a defined synthetic medium that avoids batch-to-batch composition
46 variability and induces the expression of EAEC T6SS genes [24]. In agreement with the
47 localization of T6SS MC along the cell body with an underrepresentation at the poles [15,25],
48 we observed that T6SS sheaths assemble from one position on the cell body to the opposite
49 membrane. To avoid measurements of the length of contracted sheaths or of sheaths under
50 extension, time-lapse recordings were performed and only sheaths for which the elongation
51 has been completed (i.e., when the sheath holds >1 min with the same length) were
52 considered (Figure 1*A*). The distal extremity of these extended sheaths always co-localized
53 with the TagA stopper protein (Figure 1*B*). Quantitative measurements of these T6SS tail
54 length showed low disparities, with a length mean of 0.76 ± 0.11 μm (n = 150) and a normal
55 distribution (Figure 1*C*). We thus concluded that the length of the T6SS sheath is not
56 randomly distributed, and hence that the arrest of T6SS sheath elongation is controlled. Based
57 on this conclusion, we hypothesize that T6SS sheath length might be determined by (i) the
58 number of available T6SS tail subunits, (ii) a tape measure protein, or (iii) the cell width.

59

60 **T6SS tail sheath length is not regulated by tube/sheath components stoichiometry**

61 Several reports have demonstrated that the length of some pilus-like structures is limited by
62 the number of available pilin subunits. For example, the T2SS uses a periplasmic pseudo-
63 pilus to expel the substrates in the external medium such as a piston or an Archimedes screw

64 [26]. By artificially increasing the number of pseudo-pilins, µm-long pili can be observed at
65 the cell surface, suggesting that pseudo-pilus length is determined, in part, by the number of
66 available subunits [27,28]. A strict control of the number of subunits in the cell by finely
67 tuned gene expression and protein stability levels would prevent the costly synthesis of
68 unnecessary subunits. To test whether T6SS sheath length might be controlled by the number
69 of available tail subunits, we modified the stoichiometry balance by deregulating the levels of
70 tube/sheath subunits, Hcp, TssB and TssC. TssA, which locates at the distal end of the
71 growing sheath to coordinate the assembly of the tail tube/sheath [29-31], and the TagA
72 stopper [31,32] were not included in the study as single TssA and TagA complexes are
73 responsible for promoting T6SS tail elongation and arrest. *tssB-sfGFP*, and epitope-tagged
74 *tssC* and *hcp*, were cloned into the pTrc99A vector, under the IPTG-inducible p*trc* promoter.
75 Pilot experiments showed that the production of TssB-sfGFP, TssC and Hcp can be tightly
76 controlled by varying the IPTG inducer concentrations from 0 to 250 µM in the culture
77 medium. However, although we do not know whether it results from protein aggregation or
78 stoichiometric unbalance, we noticed that IPTG concentrations higher that 50 µM yielded
79 non-functional T6SSs, as no dynamic sheath structures were observable by fluorescence
80 microscopy. Nevertheless, with IPTG concentrations ranging from 0 to 10 µM, we observed
81 an increase in TssB-sfGFP, TssC and Hcp protein levels up to ~14-18 fold (Figure 2*A*)
82 without affecting T6SS sheath formation and dynamics (Figure 2*B*). However, sheath length
83 measurement analyses did not reveal striking differences (Figure 2*B*, 2*C* and Figure S1).
84 Collectively, our results therefore argue against a direct correlation between the abundance of
85 T6SS tail subunits and T6SS sheath length.
86

87 **T6SS sheath length is not regulated by a tape measure protein**.

The length of contractile bacteriophage tails is dictated by a tape measure protein (TMP) [18-20,33,34]. Such a ruler mechanism has been also evidenced or proposed for other CISs such as antifeeding prophages and *Photorhabdus* virulence cassettes, or non-contractile structures such as T3SS injectisome needles in *Yersinia*, or the bacterial hook in *Salmonella* [21,22,35–38]. Although bacterial T6SSs have been shown to be structurally and functionally related to contractile bacteriophages [6], and contrarily to R-pyocins, AFP, PVC or ACS gene clusters [21,22,35], no gene encoding a potential TMP can be found within T6SS clusters [39]. In addition, previous experiments showing T6SS tail sheath extension in *Vibrio cholerae* spheroplasts [40] and in EAEC and *V. cholerae tagA* mutants [31,32] suggested that longer tails assemble in the cell, hence arguing against a tape measure-like mechanism. To discard this hypothesis, we sought to reposition the T6SS at the cell pole to follow the assembly of the T6SS in the long axis of the cell body. In these conditions, the presence of a TMP would cause an arrest of tail extension in the cytoplasm, whereas the tail will extend towards the opposite cell pole or until no tail subunit is available for a TMP-independent mechanism. T6SS biogenesis starts with the assembly of the membrane complex (MC) [7,15]. The T6SS MC is composed of the TssJ outer membrane lipoprotein, and TssL and TssM inner membrane proteins [14]. Its biogenesis starts with the positioning of TssJ and is pursued by the sequential recruitment of TssM and TssL [15]. The MC initially positions along the cell body with an underrepresentation at the cell pole [15,25]. To reposition T6SS MCs at the cell pole, we fused TssM to the *Bacillus subtilis* polar/septal determinant DivIVA. This approach has been successfully used to relocate the T4SS VirD4 coupling protein to the cell pole in *Agrobacterium* cells [41]. A fragment encoding the *B. subtilis divIVA* gene was inserted on the chromosome, downstream the *tssM* ATG start codon and in frame with the *tssM* coding sequence, to engineer a *divIVA-tssM* fusion. Because TssL is the last component to be recruited during MC biogenesis [15], we then imaged TssL fused to sfGFP in these cells.

Statistical analyses of sfGFP-TssL position, that hence reflects the localization of the fully-assembled T6SS MC [15], demonstrated that sfGFP-TssL forms ~32% of polar foci in presence of DivIVA-TssM, by contrast to the wild-type cells, with ~16% of polar foci (Figure 3*A*, 3*B*). Introduction of the *divIVA-tssM* fusion into *tssB-sfGFP* EAEC cells showed that few T6SS tails assemble from the pole suggesting that polar-localized MCs are less functional. However, the number of tail polymerizations starting from the cell pole was significantly increased with the relocation of the MC compared to wild-type cells. Statistical analyses showed that these extensions from the poles lead to significantly longer tails (Figure 3*C*), with a mean equal to 1.05 ± 0.42 µm (n = 75). Sheaths that crossed the entire cell body with length up to 3.5 µm (corresponding to outliers in Figure 3*C*), and capable of contraction were readily observed (Figure 3*D*). Taken together, these data demonstrate that T6SS tails could be artificially extended by relocalization of the MC at the cell pole, and hence that sheath length is not regulated by a TMP-mediated ruler mechanism.

T6SS tail sheath length is dictated by the cell width.

In all the images recorded, we observed that sheaths extend towards and stop when in contact with the opposite membrane. As the membrane mechanically defines the cell limits, one may hypothesize that the distance between the two opposite membrane positions is sufficient to determine sheath length. Indeed, the measure of the distance between the two membranes in cells analyzed in Figure 1 showed a cell width average of 0.86 µm ± 0.07, which is comparable to the sheath length (0.76 µm ± 0.11), specifically if we take into account the widths of the membranes, of the cytoplasmic portion of the MC, and of the BP [8,9,15,16]. To further investigate the impact of cell width on T6SS sheath length, we treated EAEC cells producing TssB-sfGFP with A22, a drug that causes cell shape defects by targeting the

cytoskeletal MreB protein. As expected, we observed a significant impact on cell morphology with a trend to cell rounding (Figure 4*A*). In these conditions, we observed T6SS sheaths with length varying from 0.7 to 2 µm (Figure 4*A*). However, when sheath length was plotted against cell width, a strict correlation is observed (Kendall's $\tau = 0.82$) (Figure 4*B*). In addition, the value of the slope, close to 1 ($m = 0.92$), demonstrates that sheath length is directly proportional to cell width, which is also confirmed by sheath length/cell width ratio calculations (Figure 4*C*). Similarly to wild-type cells [32], the distal extremity of these longer extended sheaths co-localized with TagA (Figure 4*D*). We therefore conclude that T6SS sheath length depends on cell width, and that T6SS sheath polymerization is arrested upon contact with the opposite membrane, likely by the TagA stopper.

Concluding remarks

In this study, we have shown that the T6SS tails in EAEC cells have a defined length. Our further analyses demonstrated that the length of the T6SS tail is not determined by a tape measure protein or by the number of available tail tube/sheath subunits, but rather by the distance between the baseplate and the opposite membrane. This mechanism contrasts with the TMP-dependent regulation found in most contractile tailed machines. However it is in agreement with the fact that no putative TMP-encoding genes are encoded on T6SS gene clusters [5,39]. In TMP-dependent contractile tails, it has been shown that a strict correlation exists between the number of TMP residues and the length of cognate sheaths [21,22]. An extrapolation for the T6SS would mean that a sheath of 0.76 µm corresponds to a TMP of ~ 5,000 amino-acids. Such a protein is not encoded within T6SS gene clusters. Finally, the observation that DivIV-mediated relocalisation of the MC to the cell pole yields extra-long sheath structures demonstrates that no TMP is involved. The assembly of extra-long sheaths

161 also suggests that the number of subunits necessary to assemble a tail tube/sheath is not
162 limiting in the bacterial cytoplasm, and hence that sheath length is not regulated by the
163 number of available tail subunits. Indeed, this hypothesis was also discarded by artificially
164 modulating the levels of T6SS tail subunits, demonstrating that it does not influence tail
165 sheath length. This results is also in agreement with the recent measurement of T6SS subunits
166 abundance demonstrating that tail tube/sheath components are not limiting in *Acinetobacter*
167 *baylyi*, *V. cholerae*, or *P. aeruginosa* cells [42]. All our observations therefore argue for an
168 arrest of sheath polymerization at the opposite membrane. This hypothesis is likely, as
169 altering the distance between the two membranes by using A22, an antagonist of the MreB
170 morphological determinant, showed a strict correlation between membrane width and sheath
171 length. We conclude that tail tube/sheath polymerization stops when it hits the opposite
172 membrane. In most cases, the assembly of the T6SS tubular structure starts perpendicular to
173 the membrane and hence, the length of the sheath correlates with the cell width. However,
174 when T6SS tail assembly starts non-perpendicularly, its polymerization will proceed until it
175 touches the opposite membrane boundary. This model is also consistent with the recent
176 identification of TagA, a membrane-bound protein that binds to the distal extremity of the
177 growing tail and stops tube/sheath polymerization in EAEC and *V. cholerae* [31,32]. However,
178 TagA is not a universal stopper as recordings of sheath dynamics of $TagA^+$ T6SS (*V.*
179 *cholerae*) or T6SSs lacking TagA (*Acinetobacter baylyi*, *P. aeruginosa* H1, *S. enterica*
180 Typhimurium, *Francisella novicida*) showed that sheaths extend to and stop at the opposite
181 membrane [40, 42-45]. It would be interesting to define how T6SS sheath polymerization is
182 stopped in bacterial species lacking TagA.

183 In conclusion, T6SS has evolved to use a mechanism of tail length control distinct
184 from other CISs. We thus propose a model in which T6SS tail length is determined by the
185 distance to the opposite membrane. In EAEC, and likely other $TagA^+$ species, proper arrest of

tail tube/sheath polymerization is mediated by the TagA stopper by binding to the TssA cap protein once the distal end of the sheath hits the opposite membrane. .

Acknowledgments

We thank Abdelrahim Zoued for constructing plasmid pKD4-YFP, Adrien Ducret for advices regarding the use of MicrobeJ, Handuo Shi, Kerwyn Casey Huang (Stanford University, USA), Daisuke Shiomi (Rykio University, Tokyo, Japan), and laboratory members for discussion, Moly Ba, Isabelle Bringer, Annick Brun, and Olivier Uderso for technical assistance, and Lydie Odu-Vilaj for encouragements. This work was funded by the Centre National de la Recherche Scientifique, the Aix-Marseille Université, and grants from the Agence Nationale de la Recherche (ANR-14-CE14-0006-02, ANR-17-CE11-0039-01), the Fondation pour la Recherche Médicale (DEQ20180339165), and the Fondation Bettencourt-Schueller to EC. YGS is supported by a doctoral fellowship from the French ministry of higher education and research. The funders had no role in study design, data collection and interpretation, or the decision to submit the work for publication.

Authors contributions

Y.G.S. and E.C. designed research; Y.G.S., T.D. and E.C. performed research; Y.G.S. performed statistical analyses; Y.G.S., T.D., and E.C. analyzed data; L.J. provided expertise and feedback; Y.G.S. and E.C. wrote the paper with contributions from T.D. and L.J.

Declaration of interests

The authors declare no competing interests.

Legend to Figures

Figure 1. Statistical measure of the EAEC T6SS sheath length. (*A*) Representative fluorescence micrograph of EAEC cells producing TssB-sfGFP and labelled with FM4-64 (upper panel, phase channel; lower panel, merge of GFP and FM4-64 channels). Scale bar, 1 μm. (*B*) Representative fluorescence micrograph of EAEC cells producing TssB-CFP and YFP-TagA, and labeled with FM4-64 (upper panel, phase channel; lower panel, merge of CFP, YFP, and FM4-64 channels). The open arrowheads point T6SS extended sheaths in contact with the TagA stopper. Scale bar, 1 μm. (*C*) Violin plot representation of the sheath length in wild-type cells. The distribution of the sheath lengths is represented by the outer shape. The bold horizontal bar represents the median value (median = 0.76 μm); the lower and upper boundaries of the internal box plot correspond to the 25th and 75th percentiles respectively; whiskers extend 1.5 times the interquartile range from the 25th and 75th percentiles. The number of measured sheaths (n=150) is indicated above.

Figure 2. T6SS tail tube/sheath subunits levels do not determine T6SS sheath length. (*A*) Western-blot analyses of tail tube/sheath component abundance. 2×10^8 cells of Δ*tssBC*Δ*hcp* cells producing TssB-sfGFP ($TssB_{sfGFP}$), 6×His-tagged TssC ($TssC_{6His}$) and FLAG-tagged Hcp (Hcp_{FLAG}) from the pTrc-B_{GFP}-C_{6H}-Hcp_F grown in presence of 0.4% of glucose or of the indicated concentration of IPTG were subjected to 12.5% acrylamide SDS-PAGE and immunodetected with anti-GFP, -His, -FLAG and -EF-Tu monoclonal primary antibodies and secondary antibodies coupled to AlexaFluor® 680. The EF-Tu cytoplasmic elongation factor is used as loading control. The increased fold values compared to the glucose condition, measured by densitometric quantification of the band signal intensities and relative to the loading control, are indicated below. Molecular weight markers (in kDa) are indicated on left. (*B-C*) Representative fluorescence microscopy recordings (*B*) and statistical analyses of sheath length measurements (*C*) of Δ*tssBC*Δ*hcp* cells producing Hcp_{FLAG}, TssB-sfGFP and

234 $TssC_{6His}$ in presence of 0.4% glucose or of the indicated concentration of IPTG, and labelled
235 with FM4-64 (left panels, phase channel; right panels, merge of GFP and FM4-64 channels).
236 Scale bar, 2 μm. In the violin plot representation of the statistical analysis, the distribution of
237 the sheath length is represented by the outer shape. The bold horizontal bar represents the
238 median; the lower and upper boundaries of the internal box plot correspond to the 25th and
239 75th percentiles respectively; whiskers extend 1.5 times the interquartile range from the 25th
240 and 75th percentiles. Outliers are shown as black dots. Statistical significance from three
241 independent assays (n= 100 for each conditions) relative to the glucose condition is indicated
242 above the plots (ns, non-significative; ***, $p < 0.001$; two-tailed Student's t-test). A
243 comparison of tail tube/sheath subunits levels and sheath lengths is shown in Figure S1.

244 **Figure 3. Sheath length is not controlled by a tape measure protein.** Representative
245 fluorescence microscopy recordings of EAEC cells producing sfGFP-TssL in WT (*A*) or
246 DivIV-TssM (*B*) cells, and labelled with FM4-64 (upper panels, phase channel; lower panels,
247 merge of GFP and FM4-64 channels). White and blue arrowheads indicate TssL foci with
248 body or polar localizations, respectively. Scale bar, 2 μm. The spatial repartition of sfGFP-
249 TssL foci is shown on right, as a projection of foci from n=152 and n=151 WT and DivIVA-
250 TssM cells, respectively, on a single cell (from blue to yellow, see heatmap color chart on
251 right of panel *A*). The percentage of sfGFP-TssL foci with polar localization is indicated
252 below. (*C*) Violin plot representation of sheath length measurements in DivIVA-TssM cells
253 producing TssB-sfGFP (red). An example of a representative microscopy field is shown in the
254 inset (scale bar, 2 μm). The distribution of sheath length in WT cells (shown in Figure 1*B*) is
255 reported in transparency for comparison (blue). The distribution of the sheath length is
256 represented by the outer shape. The bold horizontal bar represents the median value (median
257 = 0.93 μm and 0.76 μm for DivIVA-TssM and WT cells, respectively); the lower and upper
258 boundaries of the internal box plot correspond to the 25th and 75th percentiles respectively;

whiskers extend 1.5 times the interquartile range from the 25th and 75th percentiles. Outliers are shown as black dots. The number of measured sheaths (n=75) is indicated below. Statistical significance relative to WT cells is indicated above the plots (***, $p < 0.001$; one-tailed Wilcoxon's t-test). (*D*) Fluorescence microscopy time-lapse recordings of DivIVA-TssM cells producing TssB-sfGFP highlighting polar T6SS sheath assembly (white arrowhead) and contraction (blue arrowhead). Scale bar, 2 μm.

Figure 4. Cell width dictates T6SS sheath length. (*A*) Representative fluorescence micrographs of EAEC cells producing TssB-sfGFP in absence (upper panel) or in presence of the MreB inhibitor A22 (lower panel), and labelled with FM4-64 (upper panel, phase channel; lower panel, merge of GFP and FM4-64 channels). Scale bar, 2 μm. (*B*) Plot representation showing the relationship between sheath length and cell width in absence (blue) and presence of A22 (orange). The dashed line represents the mean of the WT cell width (mean = 0.87 μm). Value of the slope (m) is indicated on right. Kendall's τ = 0.82. (*C*) Dotplot of the ratios between sheath length and the width of the corresponding cell from cells grown in absence (blue) or presence of A22 (orange). Horizontal bars represent the mean in each condition. The values of the means and standard deviations are indicated above the plots. The number of analyzed cells (n) is indicated below. (*D*) Representative fluorescence micrograph of EAEC cells producing TssB-CFP and YFP-TagA in presence of the MreB inhibitor A22, and labelled with FM4-64 (left panel, phase channel; right panel, merge of CFP, YFP, and FM4-64 channels). The open arrowheads point T6SS extended sheaths in contact with the TagA stopper. Scale bar, 2 μm.

STAR METHODS

LEAD CONTACT AND MATERIALS AVAILABILITY

Further information and requests for resources and reagents should be directed to and will be fulfilled by the Lead Contact, Eric Cascales (cascales@imm.cnrs.fr). There are no restrictions to the availability of reagents.

EXPERIMENTAL MODEL AND SUBJECT DETAILS

Strains used in this study are listed in Table S1. *Escherichia coli* DH5α (New England Biolabs) or CC118λpir have been used for cloning procedures. Enteroaggregative *E. coli* (EAEC) strains used in this work are isogenic derivatives of the wild-type O3:H2 17-2 strain. The wild-type 17-2 strain and its TssB-sfGFP [46], sfGFP-TssL [15], TssB-CFP/YFP-TagA (this work), and DivIVA-TssM (this work) derivatives have been used for *in vivo* studies. *E. coli* cells were routinely grown in Lysogeny broth (LB) broth at 37°C, with aeration. For induction of the *sci1* T6SS gene cluster, cells were grown in Sci1-inducing medium [SIM: M9 minimal medium supplemented with glycerol 0.25 %, vitamin B1 200 $\mu g.mL^{-1}$, casaminoacids 40 $\mu g.mL^{-1}$, $MgCl_2$ 2 mM, $CaCl_2$ 0.1 mM, and LB (10% v/v)] [24]. Plasmids and chromosomal deletions and insertions were maintained by the addition of kanamycin (50 $\mu g.mL^{-1}$), or ampicillin (100 $\mu g.mL^{-1}$). Gene expression from pTrc99A derivative plasmids was induced at $A_{600\ nm} \approx 0.4$ by the addition of 2-10 µM of isopropyl-β-D-thio-galactopyranoside (IPTG, Sigma-Aldrich). The MreB antagonist S-(3,4-dichlorobenzyl)isothiourea hydrochloride (known as A22 [47], purchased from Sigma-Aldrich) has been added to the culture at the concentration of 10 $\mu g.mL^{-1}$ for 2 hours prior analyses. Membranes were stained with 10 $\mu g.mL^{-1}$ of the *N*-(3-triethylammoniumpropyl)-4-(6-(4-(diethylamino) phenyl) hexatrienyl) pyridinium dibromide dye (FM4-64, Molecular Probes, Life technologies).

METHOD DETAILS

Plasmid construction. All plasmids used in this study are listed in Table S2. Oligonucleotides used for plasmid construction are listed in Table S3. pTrc99A [48] and pKD4 [49] plasmid derivatives were engineered by ligation-free restriction-free cloning. PCR amplification were performed in a Biometra thermocycler using the Q5® DNA polymerase (New England Biolabs). Briefly, the fragment of interest was amplified and then used as oligonucleotides for a second PCR for amplification of the target plasmid. For construction of pTrc-B_{GFP}-C_{6His}, a fragment encoding *tssB-sfGFP* and *tssC-6×His* was amplified from EAEC 17-2 TssB-sfGFP [46] genomic DNA using primers *GGATAACAATTTCACACAGGAAACAGACCATG*AGCAGTTCGTTTCAGAATGAAATCCC and *CCCGGGTACCGAGCTCGAATTC*TTAATGGTGATGGTGATGATGCGCTTTTGCCTTCGGCATCTGC (6×His tag sequence underlined, sequence annealing on the target pTrc99A plasmid [48] italicized), and inserted into pTrc99A. The *hcp* gene was amplified from EAEC 17-2 genomic DNA using primers GCGCATCATCACCATCACCATTAAGAATTaggaggtattacaccATGGCAATTCCAGTTTATCTGTGGCTG and GGATCCCCGGGTACCGAGCTCGTTA*CTTGTCATCGTCATCTTTATAATC*CGCGGTGGTACGCTCACTCC (FLAG tag sequence italicized, sequence annealing on the target pTrc-B_{GFP}-C_{6H} plasmid underlined, Shine-Dalgarno ribosome-binding site in lower case), and inserted into pTrc-B_{GFP}-C_{6His} to yield pTrc-B_{GFP}-C_{6H}-Hcp_F. For construction of plasmid pKD4-DivIVA-Nt allowing chromosomal insertion of *divIVA* at the 5'-end of genes, the *divIVA* gene was amplified from *Bacillus subtilis* str. 168 using primers GGAACTTCGGAATAGGAACTAAGGAGGATATTCATATGCCATTAACGCCAAATGATATTCACAACAAGAC and

GCTGACATGGGAATTAGCCATGGTC*CCCTCCGCCGGCCGCTGC*TTCCTTTTCCTCA AATACAGCGTCGACTTC (3×Ala-3×Gly sequence linker italicized, sequence annealing on the target pKD4 plasmid underlined), and inserted into plasmid pKD4 [49]. For construction of plasmid pKD4-CFP-Ct allowing chromosomal insertion of *ecfp* at the 3'-end of genes, the *ecfp* gene was amplified from the pTrc99A-ecfp vector (gift from Leon Espinosa, LCB, Marseille, France) using primers GATTGCAGCATTACACGTCTTGAGCGATT*GCAGCGGCCGGCGGAGGG*GTGAGCAA GGGCGAGGAGC and GAACTTCGAAGCAGCTCCAGCCTACACTTACTTGTACAGCTCGTCCATGCCG (3×Ala-3×Gly sequence linker italicized, sequence annealing on the target pKD4 plasmid underlined), and inserted into plasmid pKD4 [49]. For construction of plasmid pKD4-YFP-Nt allowing chromosomal insertion of *eyfp* at the 5'-end of genes, the *eyfp* gene was amplified from the pCBP-EYFP vector (gift from Emmanuelle Bouveret, Institut Pasteur, Paris, France) using primers CGGAATAGGAACTAAGGAGGATATTCATATGGTGAGCAAGGGCGAGGAGC and CGGCTGACATGGGAATTAGCCATGGTC*CCCTCCGCCGGCCGCTGC*CTTGTACAGC TCGTCCATGCCGAGAG (3×Ala-3×Gly sequence linker italicized, sequence annealing on the target pKD4 plasmid underlined), and inserted into plasmid pKD4 [49]. All plasmids were verified by colony-PCR and DNA sequencing (Eurofins genomics).

Strain construction. Strains were engineered by λ-red recombination [49] using plasmid pKOBEG [50] and PCR products (oligonucleotides listed in Table S3). Briefly, a kanamycin cassette was amplified from plasmids pKD4, pKD4-DivIVA-Nt, pKD4-CFP-Ct, or pKD4-YFP-Nt, using oligonucleotides carrying 50-nucleotide extensions homologous to regions adjacent to the gene of interest. Cassette allowing deletion of the *hcp* gene was generated using the pKD4 vector template with primers

TCCCCTGCGCCGGAAGAGGGCGCATCAGAAAACATAACGGAGTAATTTTTTGTGT AGGCTGGAGCTGCTTCG and TGAAGAAAAAATAAAAATGACGGACAGGATGCCCTGTCCGTCCGGCAGAACATA TGAATATCCTCCTTAGTTCC (50-bp sequence annealing on the 5' and 3' regions of the deleted gene underlined). For chromosomal insertion of DivIVA at the *tssM* locus, the DivIVA cassette was generated using the pKD4-DivIVA-Nt vector with primers TTCTCATCCGGAGAAGAACATTTTATCAGTACTGTTACATCAGGAAACCAGAATG AATAACGATTGTGTAGGCTGGAGCTGCTTCGAAGTTCCTATAC and CACACCAATAAATACAATCCCCGGTCGCCCAAAGCGACCAGACAGACAGGCCAG TTTATTCCCTCCGCCGGCCGCTGC (50-bp sequence annealing on the 5' and 3' regions of the *tssM* ATG start codon underlined). For chromosomal insertion of CFP at the *tssB* locus, the *cfp* cassette was generated using the pKD4-CFP-Ct vector with primers CCGGCACTGAGTCAGACGCTGCGTGATGAACTGCGTGCACTGGTGCCGGAAAAG GCGGCAGCGGCCGGCGGAGGG and GCAACGTTCTTTTCTTTCTGTACAGACATCAGCATTTTCTCTCGTAATCCGTTAAA CATATGAATATCCTCCTTAGTTCCTATTCCGAAGTTCC (50-bp sequence annealing on the 5' and 3' regions of the *tssB* TAA stop codon underlined). For chromosomal insertion of YFP at the *tagA* locus, the *yfp* cassette was generated using the pKD4-YFP-Nt vector with primers CTTTTCGTCACTGTTAATCATGATTTAATACAGCAACACCGAATCTGCCGCGATTG TGTAGGCTGGAGCTGCTTCGAAGTTCCTATAC and TCCGGTAATGACCGGGGGTCACCACCGGTTTTCAGTTTCACTTCAGAAGTCCCTC CGCCGGCCGCTGC (50-bp sequence annealing on the 5' and 3' regions of the *tagA* ATG start codon underlined). Cassette amplicons were column-purified (NucleoSpin® Gel and PCR clean-up, Macherey Nagel), and 600 ng were electroporated into electrocompetent target cells

(Δ*tssBC* for Δ*hcp*; 17-2, sfGFP-TssL and TssB-sfGFP for DivIVA; 17-2 for YFP-TagA; YFP-TagA for TssB-CFP), kanamycin-resistant clones were selected and verified by colony-PCR. When possible, kanamycin cassettes were excised by the FRT-specific FLP recombinase using vector pCP20 [49].

SDS-PAGE, Western-blotting, imaging and quantification analyses. Standard methods were used for sodium dodecyl-sulfate poly-acrylamide gel electrophoresis (SDS-PAGE) and protein transfer on nitrocellulose membranes. Membranes were probed with anti-GFP (clone 7.1, Roche), anti-His (clone His1, Sigma), anti-FLAG (clone M2, Sigma), and anti-EF-Tu (clone mAb900, HyCult Biotech) monoclonal antibodies, and goat anti-mouse secondary antibodies coupled to AlexaFluor® 680 (Invitrogen). Images were recorded at λ=700 nm using an Odyssey® infrared imaging system (LI-COR Biosciences). Image analyses were performed with the ImageJ processing program using the Fiji interface [51], as previously described [52]. Briefly, the image was first converted to grayscale in .jpg format. The rectangle tool of ImageJ was used to select a rectangular area of the size corresponding to the lane width, in order to cover the minimal area to contain the whole of the largest band. The same frame was used to select each TssB, TssC, Hcp or EF-Tu band. For each selection, the number of pixels was calculated. A control region with no band was also selected to subtract the background. The number of pixels of each band, subtracted from the background, was then divided by the EF-Tu loading control intensity at the same IPTG concentration, to compensate for loading differences. The fold-change relative to the glucose sample was then calculated.

Fluorescence microscopy and statistical analyses. Cells were grown in SIM to a $A_{600\,nm} \approx$ 0.6–0.8, harvested and resuspended in fresh SIM to a $A_{600\,nm} \approx 10$. For inhibition of MreB function, cells grown in SIM were treated at $A_{600\,nm} \approx 0.3$ for 2 hours with 10 μg.mL^{-1} of A22 prior to data acquisition, as previously published [53]. For membrane staining, cells were

407 labelled with FM4-64 (10 μg.mL^{-1}) for 2 min prior to centrifugation. Concentrated cell
408 mixtures were spotted on a thin pad of SIM supplemented with 2% agarose, or 2% agarose
409 and A22 (10 μg.mL^{-1}), covered with a cover slip, and incubated for 20-30 min at room
410 temperature before microscopy acquisition. Fluorescence microscopy was performed on a
411 Nikon Eclipse Ti microscope equipped with an Orcaflash 4.0 LT digital camera (Hamamatsu)
412 and a perfect focus system (PFS) to automatically maintain focus so that the point of interest
413 within a specimen is always kept in sharp focus at all times despite mechanical or thermal
414 perturbations. All fluorescence images were acquired with a minimal exposure time to
415 minimize bleaching and phototoxicity effects. Exposure times were typically 30 ms for phase
416 contrast, 200 ms for TssB-sfGFP, 300 ms for TssB-CFP, 1 s for sfGFP-TssL, 1.5 s for YFP-
417 TagA, and 50 ms for FM4-64. The experiments were performed at least in triplicate and a
418 representative result is shown. Images were analyzed using ImageJ (http://imagej.nih.gov/ij/)
419 and the MicrobeJ v5.11y plugin (http://www.microbej.com/) [54].

420

421 **QUANTIFICATION AND STATISTICAL ANALYSIS**

422 Statistical analyses of microcopy images were performed with several representative fields
423 from at least three independent biological replicates, using Excel and the R software
424 environment. The number of measured cells or events (*n*) is indicated on each figure.
425 Differences in sheath length between groups were examined by unpaired parametric Student *t*
426 test or nonparametric Wilcoxon *t* test. Relationship between sheath length and cell width was
427 examined by Mann-Kendall test. Significance was defined by $p < 0.001$ (***) and $p < 0.0001$
428 (****).

429

DATA AND CODE AVAILABILITY

This study did not generate datasets and codes.

REFERENCES

1. Cherrak, Y, Flaugnatti, N, Durand, E, Journet, L, and Cascales, E. (2019). Structure and activity of the type VI secretion system. Microbiol. Spectrum *7*, PSIB-0031-2019.

2. Coulthurst, S. (2019). The Type VI secretion system: a versatile bacterial weapon. Microbiol. *165*, 503–515.

3. Durand, E., Cambillau, C., Cascales, E., and Journet, L. (2014). VgrG, Tae, Tle, and beyond: the versatile arsenal of Type VI secretion effectors. Trends Microbiol. *22*, 498–507.

4. Chassaing, B., and Cascales, E. (2018). Antibacterial weapons: targeted destruction in the microbiota. Trends Microbiol. *26*, 329–338.

5. Sarris, P.F., Ladoukakis, E.D., Panopoulos, N.J., and Scoulica, E.V. (2014). A phage tail-derived element with wide distribution among both prokaryotic domains: a comparative genomic and phylogenetic study. Genome Biol. Evol. *6*, 1739–1747.

6. Taylor, N.M.I., van Raaij, M.J., and Leiman, P.G. (2018). Contractile injection systems of bacteriophages and related systems. Mol. Microbiol. *108*, 6–15.

7. Brunet, Y.R., Zoued, A., Boyer, F., Douzi, B., and Cascales, E. (2015). The type VI secretion TssEFGK-VgrG phage-like baseplate is recruited to the TssJLM membrane complex via multiple contacts and serves as assembly platform for tail tube/sheath polymerization. PLoS Genet. *11*, e1005545.

8. Nazarov, S., Schneider, J.P., Brackmann, M., Goldie, K.N., Stahlberg, H., and Basler, M. (2018). Cryo-EM reconstruction of Type VI secretion system baseplate and sheath distal end. EMBO J. *37*, e97103.

9. Cherrak, Y., Rapisarda, C., Pellarin, R., Bouvier, G., Bardiaux, B., Allain, F., Malosse, C., Rey, M., Chamot-Rooke, J., Cascales, E., *et al.* (2018). Biogenesis and structure of a type VI secretion baseplate. Nat. Microbiol. *3*, 1404–1416.

10. Brunet, Y.R., Hénin, J., Celia, H., and Cascales, E. (2014). Type VI secretion and bacteriophage tail tubes share a common assembly pathway. EMBO Rep. *15*, 315–321.

11. Leiman, P.G., Basler, M., Ramagopal, U.A., Bonanno, J.B., Sauder, J.M., Pukatzki, S., Burley, S.K., Almo, S.C., and Mekalanos, J.J. (2009). Type VI secretion apparatus and

463 phage tail-associated protein complexes share a common evolutionary origin. Proc. Natl.
464 Acad. Sci. U. S. A. *106*, 4154–4159.

465 12. Basler, M., Pilhofer, M., Henderson, G.P., Jensen, G.J., and Mekalanos, J.J. (2012). Type
466 VI secretion requires a dynamic contractile phage tail-like structure. Nature *483*, 182–186.

467 13. Kudryashev, M., Wang, R.Y.-R., Brackmann, M., Scherer, S., Maier, T., Baker, D.,
468 DiMaio, F., Stahlberg, H., Egelman, E.H., and Basler, M. (2015). Structure of the Type
469 VI secretion system contractile sheath. Cell *160*, 952–962.

470 14. Aschtgen, M.-S., Gavioli, M., Dessen, A., Lloubès, R., and Cascales, E. (2010). The SciZ
471 protein anchors the enteroaggregative Escherichia coli Type VI secretion system to the
472 cell wall. Mol. Microbiol. *75*, 886–899.

473 15. Durand, E., Nguyen, V.S., Zoued, A., Logger, L., Péhau-Arnaudet, G., Aschtgen, M.-S.,
474 Spinelli, S., Desmyter, A., Bardiaux, B., Dujeancourt, A., *et al.* (2015). Biogenesis and
475 structure of a type VI secretion membrane core complex. Nature *523*, 555–60.

476 16. Rapisarda, C., Cherrak, Y., Kooger, R., Schmidt, V., Pellarin, R., Logger, L., Cascales,
477 E., Pilhofer, M., Durand, E., and Fronzes, R. (2019). In situ and high-resolution cryo-EM
478 structure of a bacterial type VI secretion system membrane complex. EMBO J. *38*,
479 e100886.

480 17. Katsura, I., and Hendrix, R.W. (1984). Length determination in bacteriophage lambda
481 tails. Cell *39*, 691–698.

482 18. Katsura, I. (1990). Mechanism of length determination in bacteriophage lambda tails. Adv.
483 Biophys. *26*, 1–18.

484 19. Abuladze, N.K., Gingery, M., Tsai, J., and Eiserling, F.A. (1994). Tail length
485 determination in bacteriophage T4. Virology *199*, 301–310.

486 20. Belcaid, M., Bergeron, A., and Poisson, G. (2011). The evolution of the tape measure
487 protein: units, duplications and losses. BMC Bioinformatics *12*, S10.

488 21. Rybakova, D., Schramm, P., Mitra, A.K., and Hurst, M.R.H. (2015). Afp14 is involved in
489 regulating the length of anti-feeding prophage (Afp). Mol. Microbiol. *96*, 815–826.

490 22. Böck, D., Medeiros, J.M., Tsao, H.-F., Penz, T., Weiss, G.L., Aistleitner, K., Horn, M.,
491 and Pilhofer, M. (2017). In situ architecture, function, and evolution of a contractile
492 injection system. Science *357*, 713–717.

493 23. Vianelli, A., Wang, G.R., Gingery, M., Duda, R.L., Eiserling, F.A., and Goldberg, E.B.
494 (2000). Bacteriophage T4 self-assembly: localization of gp3 and its role in determining
495 tail length. J. Bacteriol. *182*, 680–688.

496 24. Brunet, Y.R., Bernard, C.S., Gavioli, M., Lloubès, R., and Cascales, E. (2011). An
497 epigenetic switch involving overlapping fur and DNA methylation optimizes expression
498 of a type VI secretion gene cluster. PLoS Genet. *7*, e1002205.

25. Santin, Y.G., Camy, C.E., Zoued, A., Doan, T., Aschtgen, M.-S., and Cascales, E. (2019). Role and recruitment of the TagL peptidoglycan-binding protein during Type VI secretion system biogenesis. J. Bacteriol. *201*, e00173-19.

26. Nivaskumar, M., and Francetic, O. (2014). Type II secretion system: a magic beanstalk or a protein escalator. Biochim. Biophys. Acta *1843*, 1568–1577.

27. Sauvonnet, N., Vignon, G., Pugsley, A.P., and Gounon, P. (2000). Pilus formation and protein secretion by the same machinery in Escherichia coli. EMBO J. *19*, 2221–2228.

28. Durand, E., Bernadac, A., Ball, G., Lazdunski, A., Sturgis, J.N., and Filloux, A. (2003). Type II protein secretion in Pseudomonas aeruginosa: the pseudopilus is a multifibrillar and adhesive structure. J. Bacteriol. *185*, 2749–2758.

29. Zoued, A., Durand, E., Brunet, Y.R., Spinelli, S., Douzi, B., Guzzo, M., Flaugnatti, N., Legrand, P., Journet, L., Fronzes, R., *et al.* (2016). Priming and polymerization of a bacterial contractile tail structure. Nature *531*, 59–63.

30. Zoued, A., Durand, E., Santin, Y.G., Journet, L., Roussel, A., Cambillau, C., and Cascales, E. (2017). TssA: The cap protein of the Type VI secretion system tail. Bioessays *39*, 10.

31. Schneider, J.P, Nazarov, S., Adaixo, R., Liuzzo, M., Ringel, P.D., Stahlberg, H., and Basler, M. (2019). Diverse roles of TssA-like proteins in the assembly of bacterial type VI secretion systems. EMBO J. *12*, e100825.

32. Santin, Y.G., Doan, T., Lebrun, R., Espinosa, L., Journet, L., and Cascales, E. (2018). In vivo TssA proximity labelling during type VI secretion biogenesis reveals TagA as a protein that stops and holds the sheath. Nat. Microbiol. *3*, 1304–1313.

33. Katsura, I. (1987). Determination of bacteriophage lambda tail length by a protein ruler. Nature *327*, 73–75.

34. Boulanger, P., Jacquot, P., Plançon, L., Chami, M., Engel, A., Parquet, C., Herbeuval, C., and Letellier, L. (2008). Phage T5 straight tail fiber is a multifunctional protein acting as a tape measure and carrying fusogenic and muralytic activities. J. Biol. Chem. *283*, 13556–13564.

35. Jiang, F., Li, N., Wang, X., Cheng, J., Huang, Y., Yang, Y., Yang, J., Cai, B., Wang, Y.-P., Jin, Q., *et al.* (2019). Cryo-EM structure and assembly of an extracellular contractile injection system. Cell *177*, 370-383.e15.

36. Journet, L., Agrain, C., Broz, P., and Cornelis, G.R. (2003). The needle length of bacterial injectisomes is determined by a molecular ruler. Science *302*, 1757–1760.

37. Cornelis, G.R., Agrain, C., and Sorg, I. (2006). Length control of extended protein structures in bacteria and bacteriophages. Curr. Opin. Microbiol. *9*, 201–206.

38. Hirano, T., Yamaguchi, S., Oosawa, K., and Aizawa, S. (1994). Roles of FliK and FlhB in determination of flagellar hook length in Salmonella typhimurium. J. Bacteriol. *176*, 5439–5449.

39. Boyer, F., Fichant, G., Berthod, J., Vandenbrouck, Y., and Attree, I. (2009). Dissecting the bacterial type VI secretion system by a genome wide in silico analysis: what can be learned from available microbial genomic resources? BMC Genomics *10*, 104.

40. Vettiger, A., Winter, J., Lin, L., and Basler, M. (2017). The type VI secretion system sheath assembles at the end distal from the membrane anchor. Nat. Commun. *8*, 16088.

41. Atmakuri, K., Ding, Z., and Christie, P.J. (2003). VirE2, a type IV secretion substrate, interacts with the VirD4 transfer protein at cell poles of Agrobacterium tumefaciens. Mol. Microbiol. *49*, 1699–1713.

42. Lin, L., Lezan, E., Schmidt, A., and Basler, M. (2019). Abundance of bacterial Type VI secretion system components measured by targeted proteomics. Nat Commun. *10*, 2584.

43. Brunet, Y.R., Khodr, A., Logger, L., Aussel, L., Mignot, T., Rimsky, S., and Cascales, E. (2015). H-NS silencing of the Salmonella Pathogenicity Island 6-encoded type VI secretion system limits Salmonella enterica serovar Typhimurium interbacterial killing. Infect Immun. *83*, 2738–2750.

44. Brodmann, M., Dreier, R.F., Broz, P., and Basler, M. (2017). Francisella requires dynamic type VI secretion system and ClpB to deliver effectors for phagosomal escape. Nat Commun. *8*, 15853.

45. Liebl, D., Robert-Genthon, M., Job, V., Cogoni, V., and Attree, I. (2019). Baseplate Component TssK and spatio-temporal assembly of T6SS in *Pseudomonas aeruginosa.* Front Microbiol. *10*, 1615.

46. Zoued, A., Durand, E., Bebeacua, C., Brunet, Y.R., Douzi, B., Cambillau, C., Cascales, E., and Journet, L. (2013). TssK is a trimeric cytoplasmic protein interacting with components of both phage-like and membrane anchoring complexes of the type VI secretion system. J. Biol. Chem. *288*, 27031–27041.

47. Iwai, N., Ebata, T., Nagura, H., Kitazume, T., Nagai, K., and Wachi, M. (2004). Structure-activity relationship of S-benzylisothiourea derivatives to induce spherical cells in Escherichia coli. Biosci. Biotechnol. Biochem. *68*, 2265–2269.

48. Amann, E., Ochs, B., and Abel, K.J. (1988). Tightly regulated tac promoter vectors useful for the expression of unfused and fused proteins in Escherichia coli. Gene *69*, 301–315.

49. Datsenko, K.A., and Wanner, B.L. (2000). One-step inactivation of chromosomal genes in Escherichia coli K-12 using PCR products. Proc. Natl. Acad. Sci. U. S. A. *97*, 6640–6645.

50. Chaveroche, M.-K., Ghigo, J.-M., and d'Enfert, C. (2000). A rapid method for efficient gene replacement in the filamentous fungus Aspergillus nidulans. Nucleic Acids Res. *28*, e97.

51. Schindelin, J., Arganda-Carreras, I., Frise, E., Kaynig, V., Longair, M., Pietzsch, T., Preibisch, S., Rueden, C., Saalfeld, S., Schmid, B., *et al.* (2012). Fiji: an open-source platform for biological-image analysis. Nat. Methods *9*, 676–682.

574 52. Zoued, A., Duneau, J.-P., Durand, E., España, A.P., Journet, L., Guerlesquin, F., and
575 Cascales, E. (2018). Tryptophan-mediated dimerization of the TssL transmembrane
576 anchor is required for type VI secretion system activity. J. Mol. Biol. *430*, 987–1003.

577 53. Kawazura, T., Matsumoto, K., Kojima, K., Kato, F., Kanai, T., Niki, H., and Shiomi, D.
578 (2017). Exclusion of assembled MreB by anionic phospholipids at cell poles confers cell
579 polarity for bidirectional growth. Mol. Microbiol. *104*, 472–486.

580 54. Ducret, A., Quardokus, E.M., and Brun, Y.V. (2016). MicrobeJ, a tool for high
581 throughput bacterial cell detection and quantitative analysis. Nat. Microbiol. *1*, 16077.

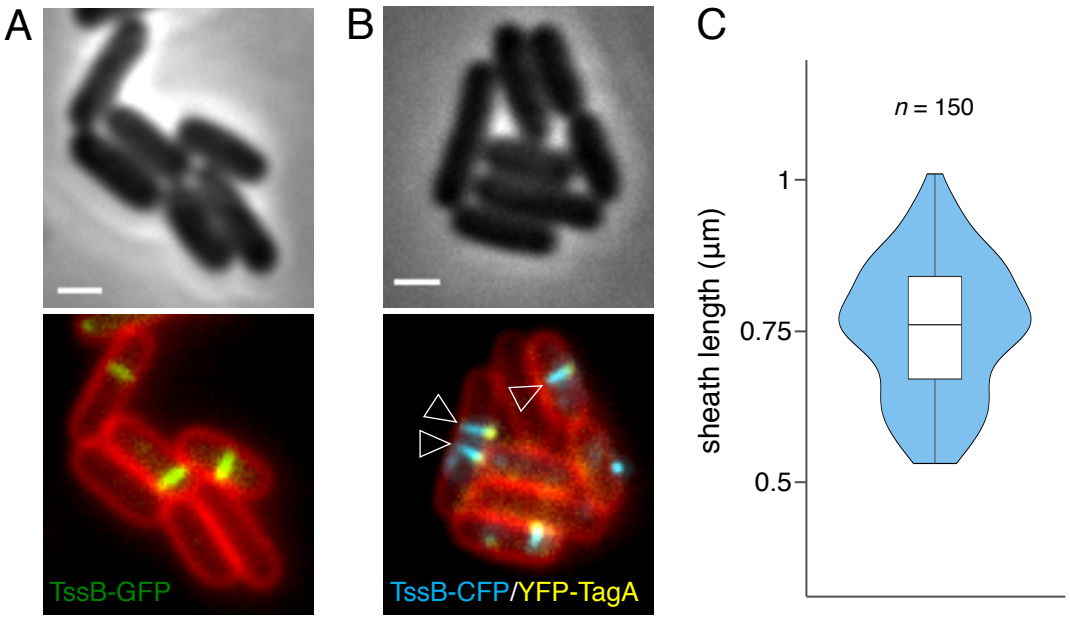

Fig. 1. Statistical measure of the EAEC T6SS sheath length. (*A*) Representative fluorescence micrograph of EAEC cells producing TssB-sfGFP and labelled with FM4-64 (upper panel, phase channel; lower panel, merge of GFP and FM4-64 channels). Scale bar, 1 µm. (*B*) Representative fluorescence micrograph of EAEC cells producing TssB-CFP and YFP-TagA, and labeled with FM4-64 (upper panel, phase channel; lower panel, merge of CFP, YFP, and FM4-64 channels). The open arrowheads point T6SS extended sheaths in contact with the TagA stopper. Scale bar, 1 µm. (*C*) Violin plot representation of the sheath length in wild-type cells. The distribution of the sheath lengths is represented by the outer shape. The bold horizontal bar represents the median value (median = 0.76 µm); the lower and upper boundaries of the internal box plot correspond to the 25th and 75th percentiles respectively; whiskers extend 1.5 times the interquartile range from the 25th and 75th percentiles. The number of measured sheaths (*n*=150) is indicated above.

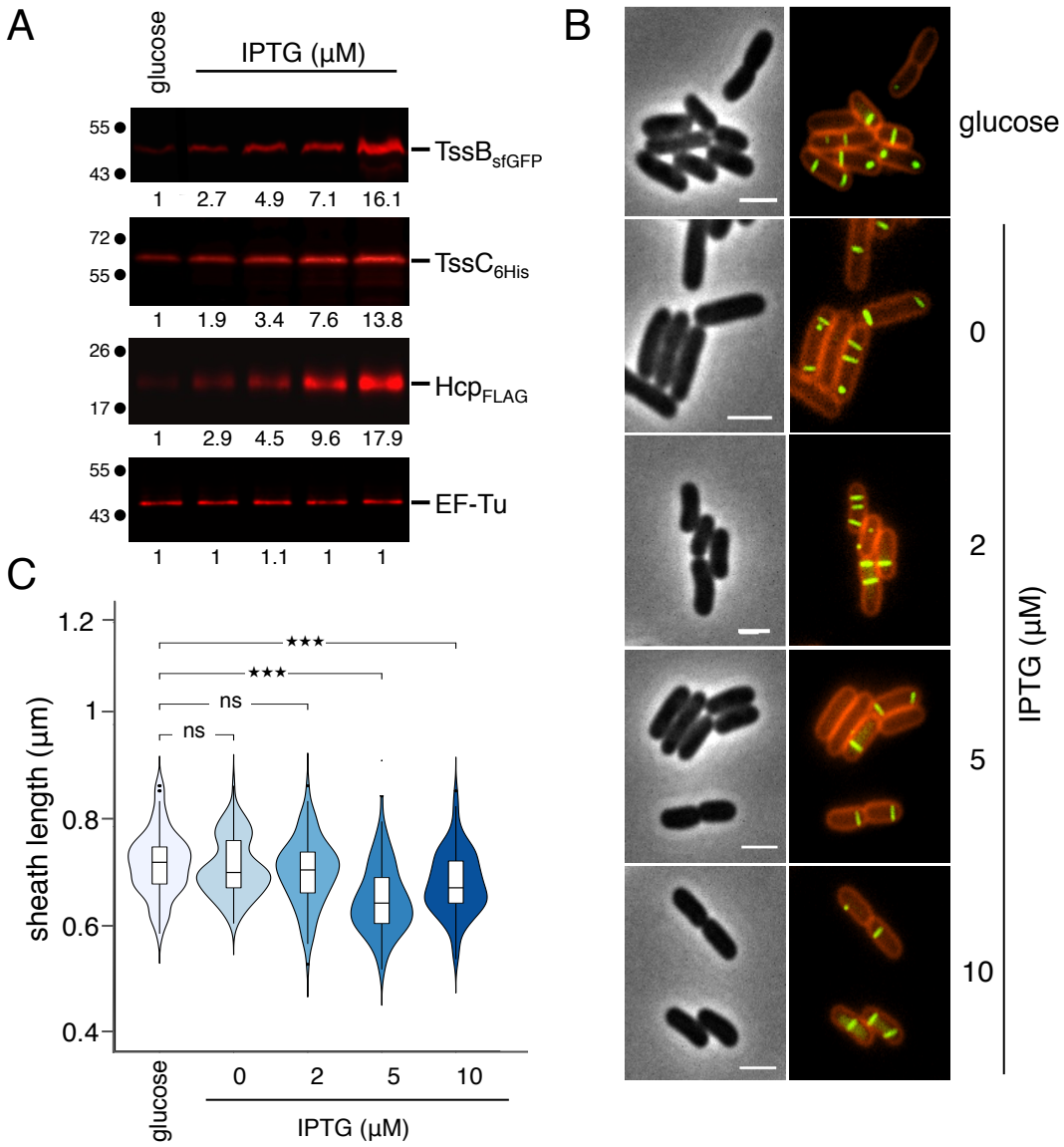

Fig. 2. T6SS tail tube/sheath subunits levels do not determine T6SS sheath length. (*A*) Western-blot analyses of tail tube/sheath component abundance. 2×10^8 cells of Δ*tssBC*Δ*hcp* cells producing TssB-sfGFP (TssB$_{sfGFP}$), 6×His-tagged TssC (TssC$_{6His}$) and FLAG-tagged Hcp (Hcp$_{FLAG}$) from the pTrc-B$_{GFP}$-C$_{6H}$-Hcp$_F$ grown in presence of 0.4% of glucose or of the indicated concentration of IPTG were subjected to 12.5% acrylamide SDS-PAGE and immunodetected with anti-GFP, -His, -FLAG and -EF-Tu monoclonal primary antibodies and secondary antibodies coupled to AlexaFluor® 680. The EF-Tu cytoplasmic elongation factor is used as loading control. The increased fold values compared to the glucose condition, measured by densitometric quantification of the band signal intensities and relative to the loading control, are indicated below. Molecular weight markers (in kDa) are indicated on left. (*B-C*) Representative fluorescence microscopy recordings (*B*) and statistical analyses of sheath length measurements (*C*) of Δ*tssBC*Δ*hcp* cells producing Hcp$_{FLAG}$, TssB-sfGFP and TssC$_{6His}$ in presence of 0.4% glucose or of the indicated concentration of IPTG, and labelled with FM4-64 (left panels, phase channel; right panels, merge of GFP and FM4-64 channels). Scale bar, 2 µm. In the violin plot representation of the statistical analysis, the distribution of the sheath length is represented by the outer shape. The bold horizontal bar represents the median; the lower and upper boundaries of the internal box plot correspond to the 25th and 75th percentiles respectively; whiskers extend 1.5 times the interquartile range from the 25th and 75th percentiles. Outliers are shown as black dots. Statistical significance from three independent assays (n= 100 for each conditions) relative to the glucose condition is indicated above the plots (ns, non-significative; ***, $p < 0.001$; two-tailed Student's *t*-test). A comparison of tail tube/sheath subunits levels and sheath lengths is shown in Fig. S1.

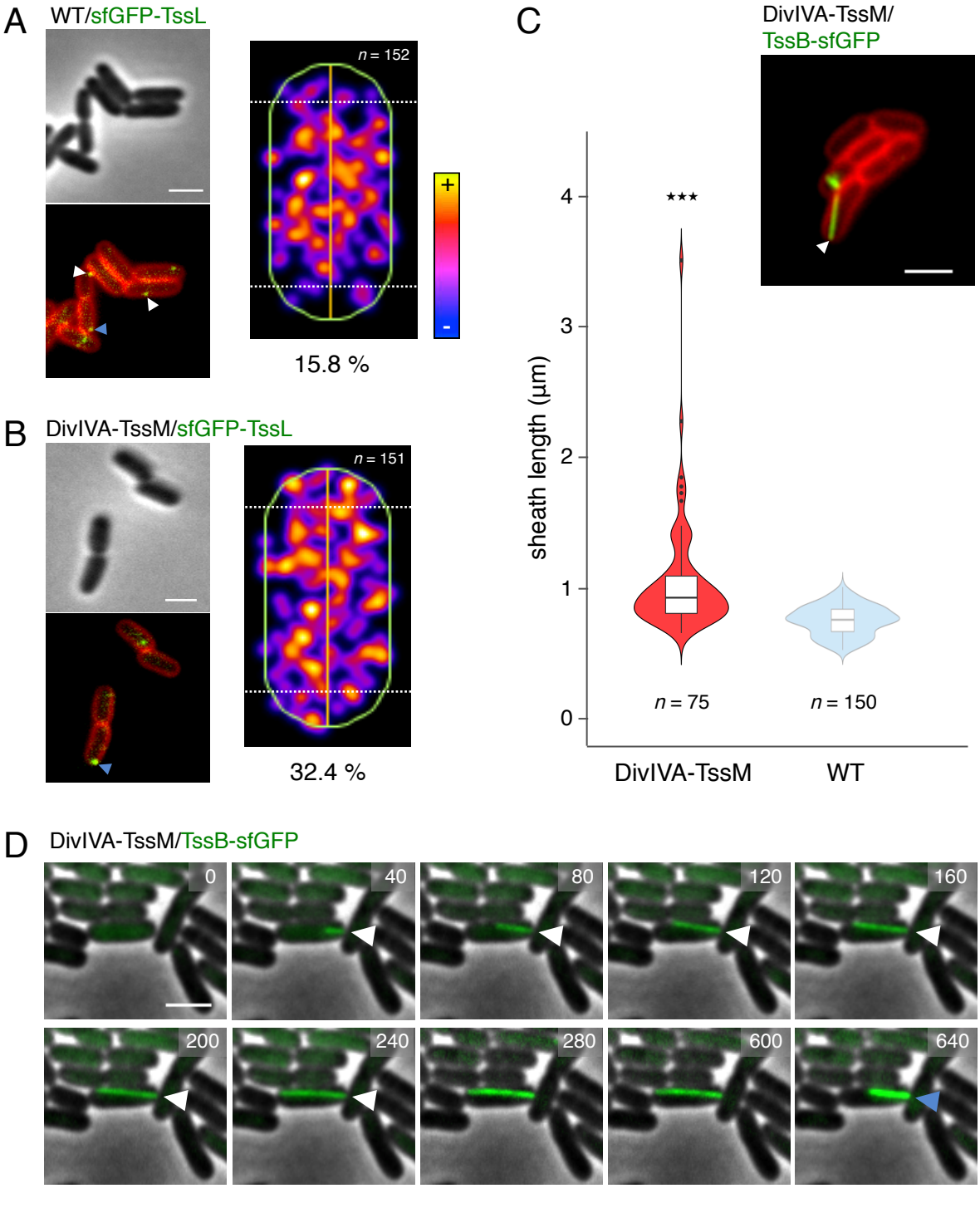
A
WT/sfGFP-TssL
n = 152
+
-
15.8 %
B
DivIVA-TssM/sfGFP-TssL
n = 151
32.4 %
C
DivIVA-TssM/
TssB-sfGFP
sheath length (µm)
0
1
2
3
4
***
n = 75
n = 150
DivIVA-TssM
WT
D
DivIVA-TssM/TssB-sfGFP
0
40
80
120
160
200
240
280
600
640

Fig. 3. Sheath length is not controlled by a tape measure protein. Representative fluorescence microscopy recordings of EAEC cells producing sfGFP-TssL in WT (*A*) or DivIV-TssM (*B*) cells, and labelled with FM4-64 (upper panels, phase channel; lower panels, merge of GFP and FM4-64 channels). White and blue arrowheads indicate TssL foci with body or polar localizations, respectively. Scale bar, 2 μm. The spatial repartition of sfGFP-TssL foci is shown on right, as a projection of foci from n=152 and n=151 WT and DivIVA-TssM cells, respectively, on a single cell (from blue to yellow, see heatmap color chart on right of panel *A*). The percentage of sfGFP-TssL foci with polar localization is indicated below. (*C*) Violin plot representation of sheath length measurements in DivIVA-TssM cells producing TssB-sfGFP (red). An example of a representative microscopy field is shown in the inset (scale bar, 2 μm). The distribution of sheath length in WT cells (shown in Fig. 1*B*) is reported in transparency for comparison (blue). The distribution of the sheath length is represented by the outer shape. The bold horizontal bar represents the median value (median = 0.93 μm and 0.76 μm for DivIVA-TssM and WT cells, respectively); the lower and upper boundaries of the internal box plot correspond to the 25th and 75th percentiles respectively; whiskers extend 1.5 times the interquartile range from the 25th and 75th percentiles. Outliers are shown as black dots. The number of measured sheaths (n=75) is indicated below. Statistical significance relative to WT cells is indicated above the plots (***, $p < 0.001$; one-tailed Wilcoxon's *t*-test). (*D*) Fluorescence microscopy time-lapse recordings of DivIVA-TssM cells producing TssB-sfGFP highlighting polar T6SS sheath assembly (white arrowhead) and contraction (blue arrowhead). Scale bar, 2 μm.

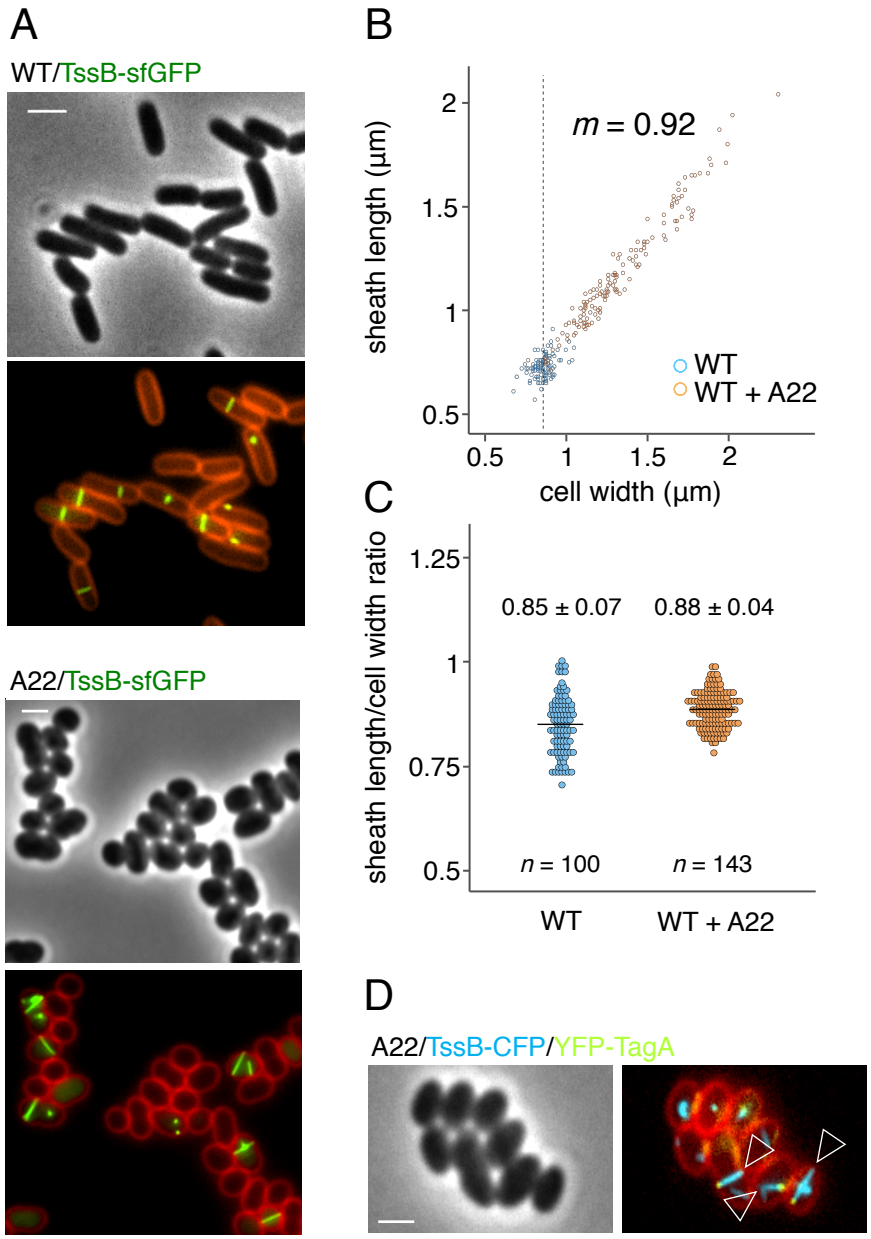

Fig. 4. Cell width dictates T6SS sheath length. (*A*) Representative fluorescence micrographs of EAEC cells producing TssB-sfGFP in absence (upper panel) or in presence of the MreB inhibitor A22 (lower panel), and labelled with FM4-64 (upper panel, phase channel; lower panel, merge of GFP and FM4-64 channels). Scale bar, 2 µm. (*B*) Plot representation showing the relationship between sheath length and cell width in absence (blue) and presence of A22 (orange). The dashed line represents the mean of the WT cell width (mean = 0.87 µm). Value of the slope (*m*) is indicated on right. Kendall's τ = 0.82. (*C*) Dotplot of the ratios between sheath length and the width of the corresponding cell from cells grown in absence (blue) or presence of A22 (orange). Horizontal bars represent the mean in each condition. The values of the means and standard deviations are indicated above the plots. The number of analyzed cells (*n*) is indicated below. (*D*) Representative fluorescence micrograph of EAEC cells producing TssB-CFP and YFP-TagA in presence of the MreB inhibitor A22, and labelled with FM4-64 (left panel, phase channel; right panel, merge of CFP, YFP, and FM4-64 channels). The open arrowheads point T6SS extended sheaths in contact with the TagA stopper. Scale bar, 2 µm.

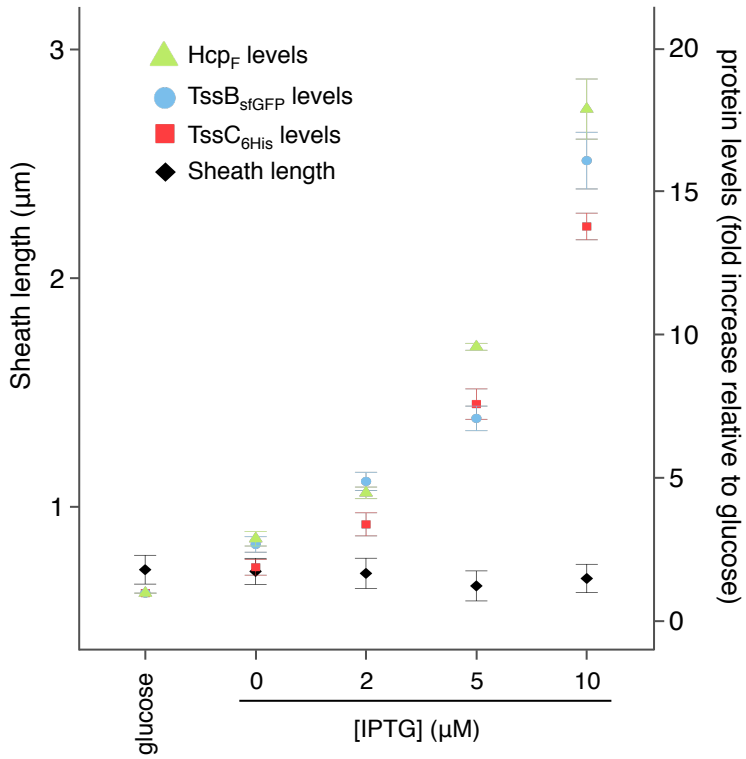

Fig. S1. T6SS tail tube/sheath subunits levels do not determine T6SS sheath length. Graph representation of the fold increase of Hcp_{FLAG} (green triangles), TssB-sfGFP (blue circles), and $TssC_{6His}$ (red squares) cellular levels as a function of the IPTG concentration (relative to the glucose condition) from Δ*tssBC*Δ*hcp* cells bearing plasmid pTrc-B_{GFP}-C_{6H}-Hcp_F. The corresponding sheath lengths are indicated with black diamonds. The mean and standard deviations from three independent experiments are shown.